Generating high spatiotemporal resolution LAI based on MODIS/GF-1 data and combined Kriging-Cressman interpolation

Liu Zhenhua[1,2,3,4,5], Huang Rugen[1,2,3,4,5,6], Hu Yueming[1,2,3,4,5*], Fan Shudi[1,2,3,4,5], Feng Peihua[1,2,3,4,5]

(1. *College of Natural Resources and Environment, South China Agricultural University, Guangzhou 510642, China*; 2. *Guangdong Provincial Key Laboratory of Land Use and Consolidation, Guangzhou 510642, China*; 3. *Guangdong Province Engineering Research Center for Land Information Technology, Guangzhou 510642, China*; 4. *Key Laboratory of the Ministry of Land and Resources for Construction Land Transformation, Guangzhou 510642, China*; 5. *Guangzhou Surveying and Mapping Geographic Information Industry Engineering Technology Research Center, Guangzhou 510642, China*; 6. *Pearl River Comprehensive Technology Center (Information Center) of Pearl Water Resources Commission, Guangzhou, 510611, China*)

Abstract: Generation of high spatial and temporal resolution LAI (leaf area index) products is challenging because higher spatial resolution remotely sensed data usually have coarse temporal resolutions and vice versa. In this study, a novel method that combining Kriging interpolation and Cressman interpolation was proposed to generate high spatial and temporal resolution LAI products by fusing Moderate Resolution Imaging SpectroRadiometer (MODIS) characterized by coarse spatial resolution and high temporal resolution and Gaofen-1 (GF-1) with fine spatial resolution and coarse temporal resolution. This method was applied to the Huangpu district of Guangzhou, Guangdong, China. The results showed that compared to field observation, the predicted values of LAI had an acceptable accuracy of 73.12%. Using Moran's I index and Kolmogorov-Smirnov tests, it was found that the MODIS data were spatially auto-correlated and characterized by normal distributions. Scaling down the 1 km× 1 km spatial resolution MODIS products to a spatial resolution of 30 m×30 m using point-Kriging resulted in a precision of 79.38% compared to the results at the same spatial resolution derived from an 8 m×8 m spatial resolution GF-1 image by scaling up using block-Kriging. Moreover, the regression models that accounts for the relationship between NDVI (Normalized Difference Vegetation Index) and LAI based on MODIS data obtained the determination coefficients ranging from 0.833 to 0.870. Finally, the data fusion and interpolation of MODIS and GF-1 data using Cressman method generated high spatial and temporal resolution LAI maps, which showed reasonably spatial and temporal variability. The results imply that the proposed method is a powerful tool to create high spatial and temporal resolution LAI products.

Keywords: data fusion, MODIS, GF-1, LAI, spatiotemporal resolution, spatial interpolation, remote sensing
DOI: 10.3965/j.ijabe.20160905.1777

Citation: Liu Z H, Huang R G, Hu Y M, Fan S D, Feng P H. Generating high spatiotemporal resolution LAI based on MODIS/GF-1 data and combined Kriging-Cressman interpolation. Int J Agric & Biol Eng, 2016; 9(5): 120－131.

1 Introduction

LAI (leaf area index) is one of the extremely important parameters in process-based models that indirectly quantify the material and energy exchange of land surface with plant boundary layer[1,2]. Accurate measurement of LAI is critical for assessing vegetation growth and carbon sequestration that maintains ecological balance. As a traditional method, field point measurement cannot practically satisfy the diverse needs for retrieving LAI at various spatial and temporal scales. Moreover, the field measurement based method is labor intensive and expensive. In contrast, remote sensing techniques are used to rapidly monitor the dynamics of LAI at regional scales because of their spatially explicit measurements

Received date: 2015-05-14 **Accepted date:** 2016-03-08
Biographies: Liu Zhenhua, Associate Professor, research interests: quantitative remote sensing, Email: greenmountain@163.com; **Huang Rugen**, Master, research interests: quantitative remote sensing, Email: oscargen@163.com; **Fan Shudi**, Master, research interests: land use engineering, fsd_1990@126.com; **Feng Peihua**, Master, research interests: quantitative remote sensing, Email: 342045594@qq.com.
***Corresponding author: Hu Yueming**, Professor, College of Natural Resources and Environment, Guangzhou 510642, China. Tel: +86-020-85288307, Email: ymhu@163.com.

and almost real-time dynamics monitoring as well as a relatively low cost.

Global LAI products have been provided by using satellite observations on a routine basis, such as Medium Resolution Imaging Spectrometer (MERIS), Multi-angle Imaging SpectroRadiometer (MISR), Polarization and Directionality of Earth Reflectance (POLDER) and widely used Moderate Resolution Imaging SpectroRadiometer (MODIS). Most of these products have medium or coarse spatial resolutions and limited estimation precision of crops and vegetation parameters such as vegetation structure due to the existence of mixed pixels. Though high spatial resolution images can be acquired and utilized to reduce the effects of mixed pixels, it is often found that such data do not fully meet the requirements of deriving fine spatial resolution LAI products because of their coarse temporal resolutions compared to the moderate spatial resolution products such as MODIS LAI.

On the other hand, such high spatial resolution LAI products can also be obtained by scaling down moderate spatial resolution MODIS LAI data and then combining them with the information provided by fine spatial resolution images such as those from Gaofen-1(GF-1) satellite with a spatial resolution of 8 m. So far, various downscaling algorithms have been developed and can be grouped into pixel-based methods and object-oriented methods[3-6]. The object-oriented methods are the procedures of texture extraction and image segmentation, and are complicated. Relatively, the pixel-based methods are simple and they integrate the image information based on a window of $n \times n$ pixels. The implementation can be achieved using commonly used algorithms such as local average, center point, nearest neighbor, bilinear interpolation and cubic convolution[6,7]. But, these methods rely solely on spectral data of images, and do not take into account of image texture and structure, which limit the precision of the downscaling transformation[8]. In comparison with the aforementioned methods, Kriging is a spatial interpolation or geostatistical method that can produce predictions of unobserved locations using observed values at nearby locations. Kriging weights the observed values for each unknown location according to their distances from the unknown location and spatial auto-correlation of an interest variable. Kriging estimator is unbiased and its Kriging Variance is minimized. Many studies have indicated that the geostatistical method is promising to study the spatial structure of continuous random variables[9-16]. The predictions obtained by Kriging are more accurate than those by traditional spatial interpolation methods[17].

This study aimed at developing and accessing a novel method that could be used to generate high spatial resolution LAI products by fusing the relevant MODIS products and GF-1 images. In this way, MODIS products should have fine temporal resolutions and GF-1 images should have fine spatial resolution. This method was developed based on the idea of data fusion and scale transformation by combining Kriging and Cressman spatial interpolation methods.

2 Materials and methods

2.1 Study area and data

This study was conducted in the central part of Huangpu district suburb, Guangzhou, Guangdong Province, China, and shown with an 8 m×8 m spatial resolution GF-1 true color composite image (Figure 1). The area is about 930 km^2 with an average altitude of 120 m (center longitude 23°15'14"N, latitude 113°26'55"E). The climate is humid subtropical monsoon climate, characterized by warm winters, hot summers, little frost and snow, sufficient rain and sunshine with an annual average temperature of 22ºC. The monthly average precipitation is 280-300 mm. The main vegetations in the area are subtropical evergreen broadleaf forests and common crops.

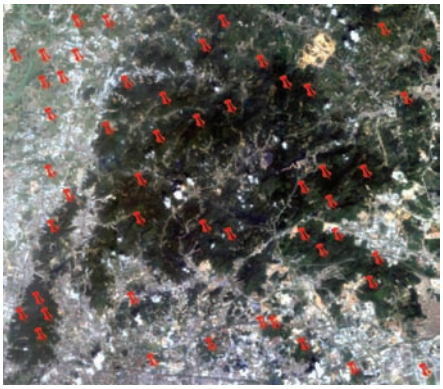

Figure 1 The 8 m spatial resolution GF-1 true color composite image of the study area and the spatial distribution of 50 sample plots

An 8 m spatial resolution GF-1 image with three visible bands (0.45-0.52 μm, 0.52-0.59 μm, 0.63 -0.69 μm) and one near-infrared band (0.63-0.69 μm) was acquired on October 1, 2013. The GF-1 image does not contain LAI data, but the image bands can be used to calculate NDVI. GF-1 is the first one of high-resolution optical earth observation satellites series of China National Space Administration (CNSA) and provides data for service and decision making of land planning and management and agricultural disaster monitoring, resource and environmental safety and so on. Geometric correction of GF-1 was conducted using a total of 20 ground control points and least-squares transformation with a root mean square error (RMSE) of less than 0.5 pixel.

The 1 km spatial resolution MODIS LAI product (MOD15A2) and reflectance product (MOD13A2) dated September 30, 2013, were also collected. The products from MODIS Terra and Aqua satellites have a high temporal resolution and are an important data source of LAI and other parameters of terrestrial ecosystems[18]. To improve the image quality, the MODIS products were geometrically corrected using MODIS Tool software. Atmospheric corrections of both GF-1 and MODIS data were carried out using FLAASH model[19]. Moreover, the MODIS products were geometrically co-registered to the GF-1 image using the coordinates of the corner points of GF-1 image.

In order to obtain a high spatial resolution GF-1 LAI product dated October 1, 2013, we carried out a LAI synchronous observation experiment when GF-1 satellite overpassed the study area. In the experiment, a total of 50 sample plots in farm lands, grass lands and broadleaf forests were selected to estimate LAI. The sample plots were shown with several vegetation types, including rice, corn and other crops, broadleaf forests such as eucalyptus and fruit trees. Each of the sample plots had an area of 30 m×30 m. The plant canopy analyzer (LAI-2000) was selected to collect field observations of LAI for the vegetation canopy types at systematically sampled five points along a diagonal line within each sample plot.

2.2 Methods

Before this study, various experiments were conducted to find an optimal spatial resolution of LAI product for the study area and the obtained results indicated that the optimal spatial resolution was 30 m. In this study, MODIS LAI products were thus scaled down from the spatial resolution of 1 km to the spatial resolution of 30 m×30 m using a point-Kriging interpolation, while a block-Kriging was applied to scale up the GF-1 data from the spatial resolution of 8 m×8 m to the spatial resolution of 30 m. Moreover, regression models were developed for various vegetation canopy types to explain the relationships between LAI and NDVI based on MODIS products and then utilized to derive GF-1 LAI data. Finally, the data fusion of MODIS and GF-1 products was conducted to generate high resolution and temporally and spatially continuous LAI products using Cressman interpolation.

2.2.1 Point-Kriging for scaling down MODIS LAI data

Kriging is a spatial interpolation method that can be used to produce predictions of unobserved locations using the observations results at nearby locations. The predicted values were calculated as the weighted means of the values from the nearby sampled points. The unbiased estimator for ordinary point-Kriging is[20]:

$$Z_0 = \sum_{i=1}^{n} \lambda_i Z_i \tag{1}$$

where, Z_1, Z_2,..., Z_n is the observed values of MODIS LAI data; Z_0 denotes the predicted value of LAI for a location; λ_i (i = 1, 2, ..., n) is the weight for the i^{th} pixel and can be derived using following equation:

$$\begin{bmatrix} \gamma_{11} & \cdots & \gamma_{1n} & 1 \\ \vdots & \ddots & \vdots & 1 \\ \gamma_{n1} & \cdots & \gamma_{nn} & 1 \\ 1 & \cdots & 1 & 0 \end{bmatrix} \cdot \begin{bmatrix} \lambda_1 \\ \vdots \\ \lambda_n \\ \mu \end{bmatrix} = \begin{bmatrix} \gamma_{10} \\ \vdots \\ \gamma_{n0} \\ 1 \end{bmatrix} \tag{2}$$

where, γ_{ij} (i, j = 1, 2, ..., n) is the semivariance between pixels i and j from semivariogram derived using MODIS data; μ is Lagrangrian coefficient. An empirical semivariogram $\gamma(h)$ is defined as[21]:

$$\gamma(h) = \frac{1}{2N(h)} \sum_{i=1}^{N(h)} \left[Z(x_i) - Z(x_i + h) \right]^2 \tag{3}$$

where, $N(h)$ denotes the number of data pairs given a direction and distance h between pixels x_i and x_i+h; $Z(x_i)$ and $Z(x_i+h)$ are the observations at locations x_i and x_i+h, respectively.

With Kriging, it is assumed that sample point data are spatially auto-correlated. The spatial auto-correlation explains the spatial variability of data. It is also assumed that the data have a normal distribution. There are several methods that can be used to test the spatial auto-correlation of data, including Moran's I index, Geary Ratio, Cliff-Ord statistic and so on[25]. In this study, Moran's I was used to test the spatial auto-correlation of MOIDS data. Moreover, Kolmogorov-Smirnov test was applied to test the MODIS data for the normality at a significance level of 0.05.

2.2.2 Block-Kriging for scaling up GF-1 data

In contract with point-Kriging, block-Kriging refers to the case where both the prediction and measurement supports are blocks rather than points[22]. Based on the research of Goovaerts[20], the unbiased estimator for an unobserved block is:

$$Z_B = \sum_{i=1}^{n} \lambda_i \cdot Z_i \tag{4}$$

where, λ_i (i = 1, 2, ..., n) is the weight derived using the following equation:

$$\begin{bmatrix} \gamma_{11} & \cdots & \gamma_{1n} & 1 \\ \vdots & \ddots & \vdots & 1 \\ \gamma_{n1} & \cdots & \gamma_{nn} & 1 \\ 1 & \cdots & 1 & 0 \end{bmatrix} \cdot \begin{bmatrix} \lambda_1 \\ \vdots \\ \lambda_n \\ \mu \end{bmatrix} = \begin{bmatrix} \overline{\gamma}_{1x} \\ \vdots \\ \overline{\gamma}_{nx} \\ 1 \end{bmatrix} \tag{5}$$

where, $\overline{\gamma}_{1x}$, ..., $\overline{\gamma}_{nx}$ are the within-block semivariance and are defined as:

$$\overline{\gamma}_{ix} = \frac{1}{|A_x|} \sum_{i=1, j \in x}^{n} \gamma_{ij} \tag{6}$$

where, $|A_x|$ represents the area of the block.

2.3 Cressman method for retrieving high spatial and temporal resolution LAI

Cressman interpolation is a computationally fast method, and it linearly combines the residuals between predicted values and observed values or reference values. The residuals are weighted depending on the distance between predicted and observed locations. This method is appropriate for generating predictions. It is stable when the spatial resolution of image data used is higher than the model grid resolution. The predictions of Cressman analysis can be calculated according to following equation[23]:

$$x_a(r_i) = x_b(r_i) + \frac{\sum_{j=1}^{n} \varphi(r_i, r_j)\left[x_0(r_j) - x_b(r_j)\right]}{\sum_{j=1}^{n} \varphi(r_i, r_j)} \tag{7}$$

where, n is the number of image pixels for different kinds of vegetation; r_i and r_j represent the model and image data grid points, respectively; x_b is the background value considered when the MODIS LAI is interpolated in this study; x_0 is the observation data from MODIS LAI when a GF-1 LAI value x_a is predicted. The weight function $\varphi(r_i, r_j)$ is written as:

$$\varphi(r_i, r_j) = \max\left(0, \frac{R^2 - d_{ij}^2}{R^2 + d_{ij}^2}\right) \tag{8}$$

where, d_{ij} is the distance between points r_i and r_j; R is the influence radius.

With Cressman method, the influence radius R and the shape of weight function $\varphi(r_i, r_j)$ have to be selected for different kinds of vegetation. The shape of the weight function determines how the image data influence the model. To improve the precision of Cressman analysis, a landscape index was introduced to acquire the influence radius R in this study based on the following equation:

$$R_i = \sqrt{\frac{\overline{A_i}}{\pi}} \cdot D_i \cdot (1 - F_i) \tag{9}$$

where, represents the mean patch area for a vegetation type; F_i is the fragment index; D_i is the landscape dominance index based on Equation (10)[24]:

$$D_i = \log_2(m) + \sum_{i=1}^{m} (p_i) \log_2 p_i \tag{10}$$

where, m is the total number of land cover categories in the study area; p_i is the proportion of the grid cells for a land cover type in the landscape.

The landscape dominance index measures the deviation between the landscape diversity and the greatest diversity.

Because only one GF-1 image was used in this study, LAI_i on the ith day for each pixel must be adjusted using the following equation:

$$LAI_i = \frac{46 - W_i}{46} \cdot L \tag{11}$$

where, W_i represents the date difference; L is the LAI difference between the GF-1 LAI value on October 1 and the 34th MODIS LAI. Based on the MODIS data used in

this study, the constant in Equation (11) was set up as 46, which equals to the total number of MODIS images within a year.

3 Results

3.1 Spatial downscaling of MODIS products

The results of Moran's I index from MODIS data are shown in Figure 2. The values of Moran's I index for red band, near-infrared band, NDVI and LAI were 0.722, 0.703, 0.774 and 0.655, respectively. The values of z-score for red band, near-infrared band, NDVI and LAI were 32.69, 31.84, 34.99 and 29.65, respectively. These indicated that the MODIS data were spatially clustered or auto-correlated and there was a probability of less than 1% that the spatially clustered patterns could be the results of random chance.

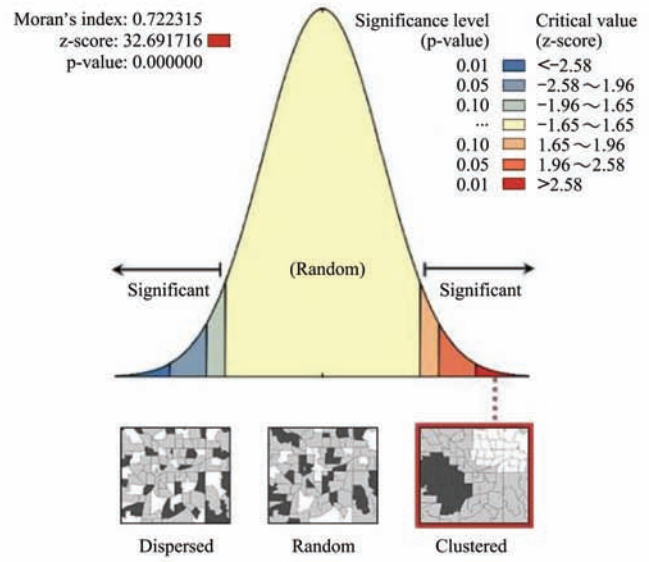

a. Moran's I for red band

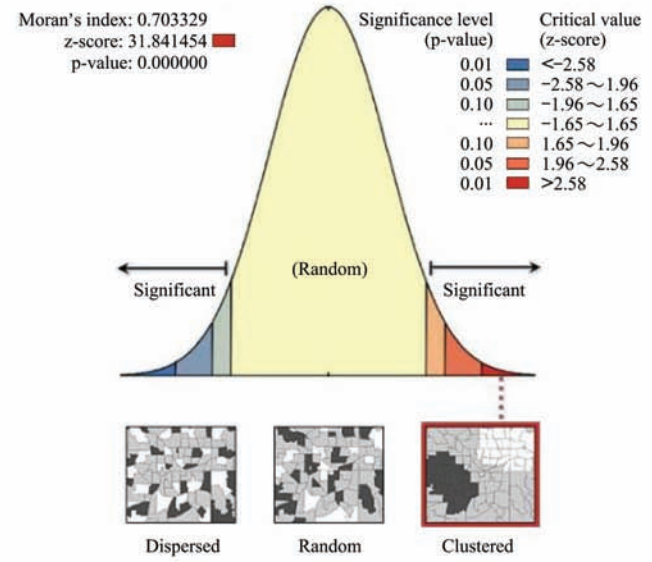

b. Moran's I for near-infrared band

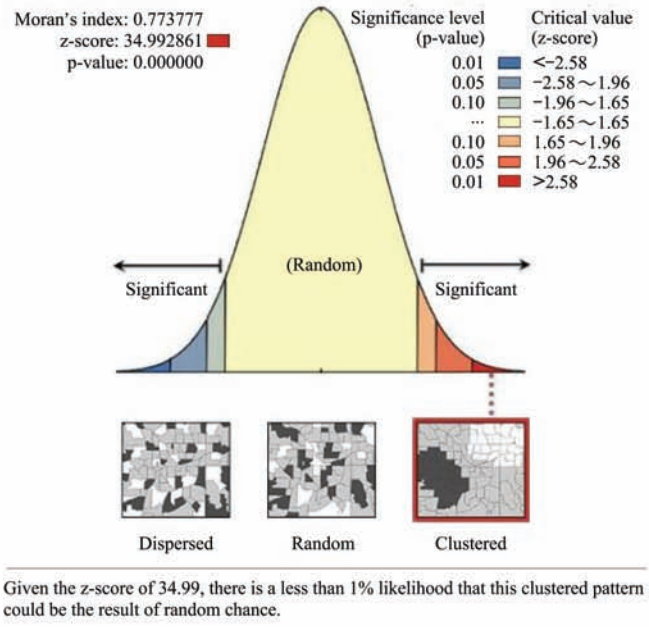

c. Moran's I for NDVI

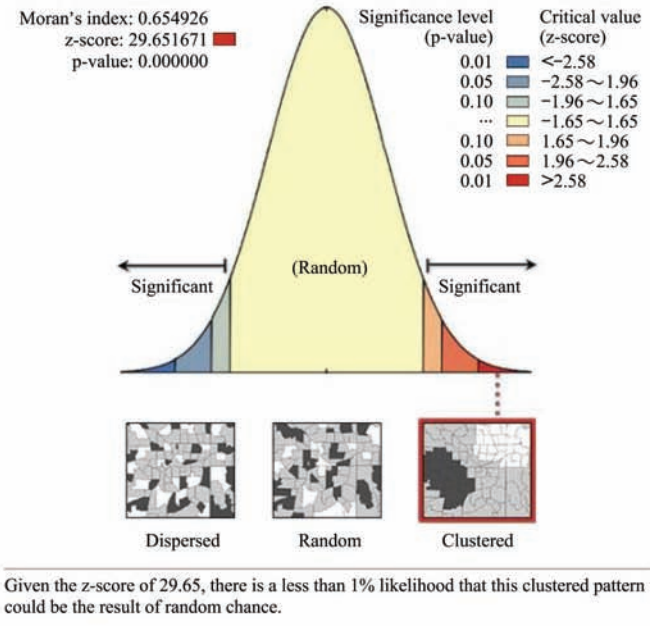

d. Moran's I for LAI

Figure 2 Results of Moran's I index for MODIS data

The results of Kolmogorov-Smirnov test for the normality of MODIS data are shown in Table 1. All the probabilities were greater than 0.05[26], which implied that the hypotheses of normal distribution for red band, near-infrared band and LAI were acceptable. NDVI had a log normal distribution. Thus, the MODIS products

could be scaled down from a coarser spatial resolution to a finer one using Kriging.

Table 1 Kolmogorov-Smirnov test for MODIS data

Normal distribution test	Red band	Near-infrared band	NDVI	LAI
Probability	0.120	0.097	0.068	0.074
Distribution	normal	normal	Logarithmic normal	normal

According to the spatial resolution of MODIS LAI product, set h=920 m, the experimental semivariograms were computed for all directions using MODIS LAI image and then fitted using spherical, exponential, Gaussian and void hole effect model. As an example, the results for LAI were shown in Figure 3.

The calculations and model fittings were also conducted for MODIS red band, near-infrared band and NDVI. The part results of the semivariogram model parameters, including nugget, sill and range, are listed in Table 2.

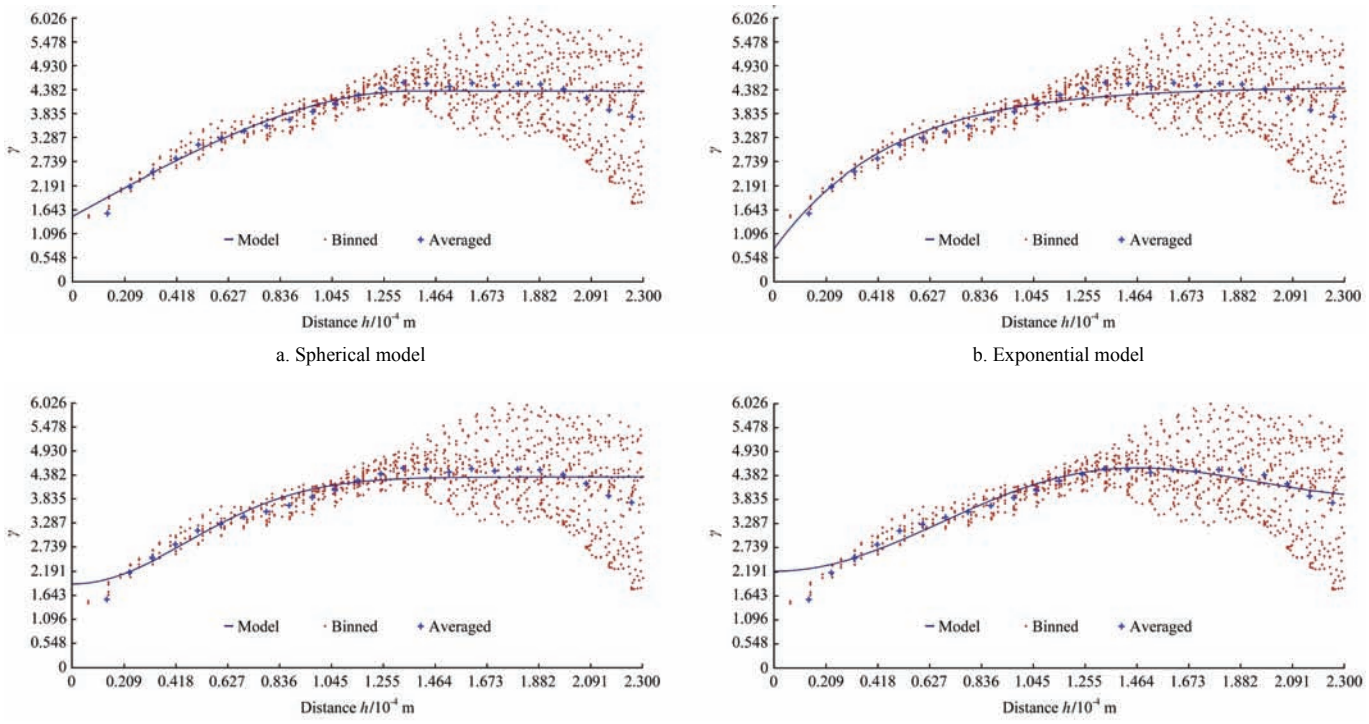

a. Spherical model b. Exponential model

c. Gaussian model d. Void hole effect model

Figure 3 Omnidirectional experimental semivariograms and their models of MODIS LAI product

Table 2 Parameters of semivariogram models fitted to MODIS NDVI and LAI data

Data	Model	Nugget (C_0)	Sill (C_0+C)	$C_0/(C_0+C)$/%	Range/km	Average of residuals	RMSE
NDVI	Spherical	7.90×10^{-3}	3.33×10^{-2}	23.69	21.76	-1.98×10^{-5}	8.22×10^{-2}
	Exponential	3.04×10^{-3}	3.38×10^{-2}	9.00	23.00	-2.71×10^{-5}	7.54×10^{-2}
	Gaussian	1.19×10^{-3}	3.38×10^{-2}	35.48	18.70	1.51×10^{-4}	9.10×10^{-2}
	Void hole effect	1.12×10^{-3}	2.82×10^{-2}	39.79	23.00	6.09×10^{-5}	9.09×10^{-2}
LAI	Spherical	1.50	4.35	34.48	13.75	2.72×10^{-4}	1.23
	Exponential	0.76	4.44	17.12	14.10	-4.89×10^{-4}	1.18
	Gaussian	1.91	4.34	44.00	11.41	1.31×10^{-4}	1.28
	Void hole effect	2.21	4.14	53.38	20.58	3.64×10^{-3}	1.29

The spatial auto-correlation of MODIS products was ranked according to the nugget-to-sill ratio, that is, $C_0/(C_0+C)$)[27]. When the ratio<25%, 25%<it<75%, and it>75%, the variables showed a strong, moderate and weak spatial auto-correlation, respectively[25]. Moreover, the smaller the RMSE, the more accurate the model fitted. Thus, the exponential model could obtain the greatest accuracies for all the MODIS products, expressed as:

$$\gamma_{red}(h) = 1.55\times10^{-4} + 6.51\times10^{-4}\cdot(1-e^{-\frac{h}{2.3\times10^4}}) \quad (13)$$

$$\gamma_{nir}(h) = 2.05\times10^{-4} + 9.6\times10^{-4}\cdot(1-e^{-\frac{h}{2.3\times10^4}}) \quad (14)$$

$$\gamma_{NDVI}(h) = 3.04\times10^{-3} + 3.08\times10^{-2}\cdot(1-e^{-\frac{h}{2.3\times10^4}}) \quad (15)$$

$$\gamma_{LAI}(h) = 0.76 + 3.68 \cdot (1 - e^{-\frac{h}{1.41\times10^4}}) \quad (16)$$

In Figure 4, the 1 km×1 km spatial resolution MODIS products were scaled down to a spatial resolution of 30 m×30 m using Kriging based on the semivariograms Equations (13)-(16) for red band (Figure 4a vs. 4b), near-infrared band (Figure 4c vs. 4d), NDVI (Figure 4e vs. 4f) and LAI (Figure 4g vs. 4h). The downscaled images had the spatial distributions similar to those at the 1 km× 1 km spatial resolution, but they looked more smoothed and detailed.

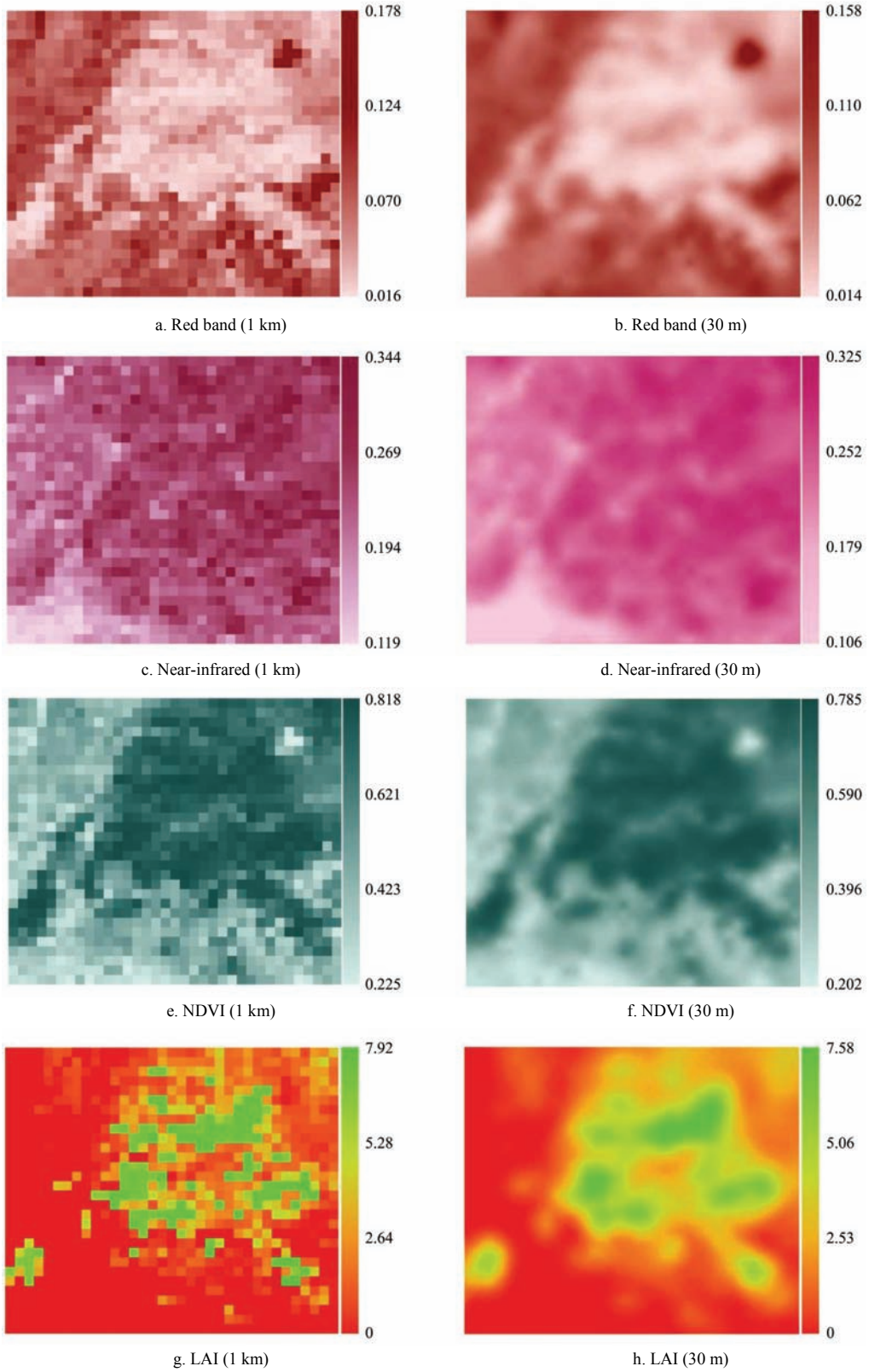

Figure 4 Spatial resolution MODIS products (1 km, left) vs. downscaled spatial resolution images using Kriging (30 m, right)

3.2 Accuracy assessment

3.2.1 Indirect assessment

Numerous studies have been reported on the strong linear relationship between NDVI and LAI[16,28,29]. The precision of NDVI predictions can be thus used as an indirect indicator for the precision of LAI prediction. Block-Kriging was first applied to scale up the 8 m×8 m spatial resolution GF-1 NDVI data to a spatial resolution of 30 m×30 m in Figure 5. In this study, the precision of NDVI predictions were obtained by calculating and using the standard error of predicted NDVI values from the downscaled MODIS product as a percentage of estimated NDVI from the up-scaled GF-1 data[30]. In Figure 6, the average precision was more than 79.38% with an average error coefficient of 20.62% for NDVI.

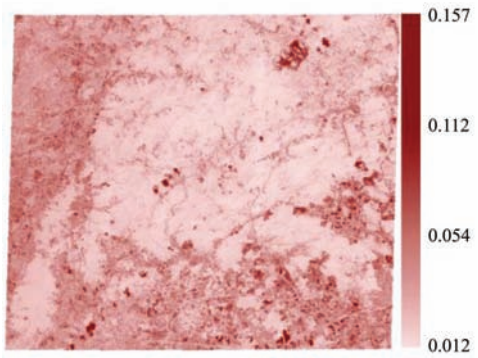

a. Red band

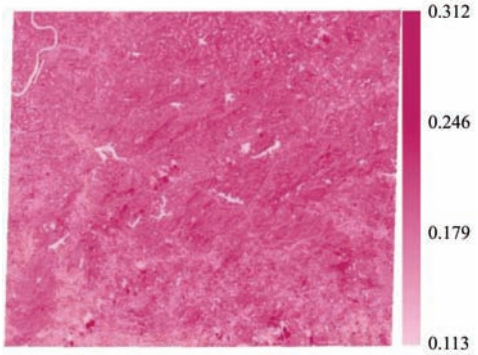

b. Near-infrared band

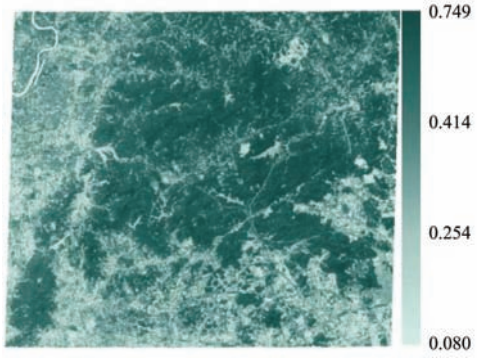

c. NDVI

Figure 5 Spatial resolution GF-1 products (8 m)

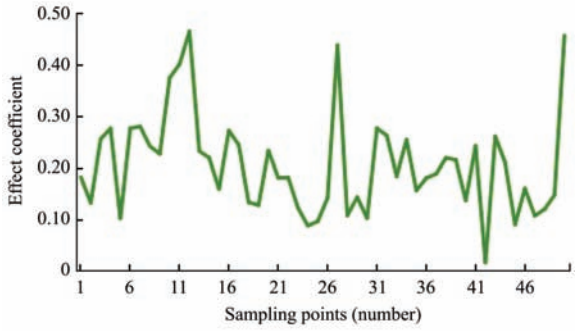

Figure 6 Error coefficient of NDVI calculated as an absolute value of prediction minus reference divided by the reference based on sampled points

3.2.2 Accuracy assessment of LAI based on field observations

The LAI estimates from the downscaled MODIS LAI data were validated using field observations in Figure 7. An accuracy of 73.12% was obtained for the predictions of LAI, implying that using Kriging, downscaling MODIS LAI from 1 km×1 km spatial resolution to 30 m×30 m was appropriate.

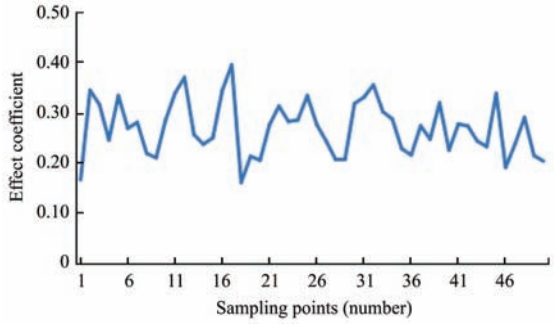

a. Farmland

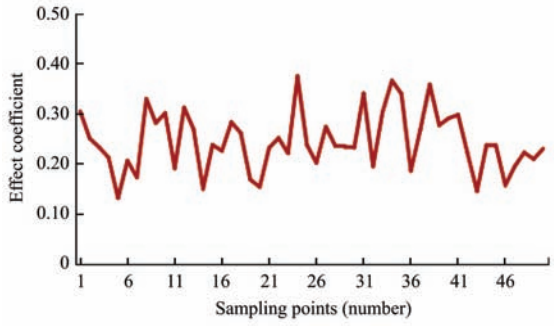

b. Grassland

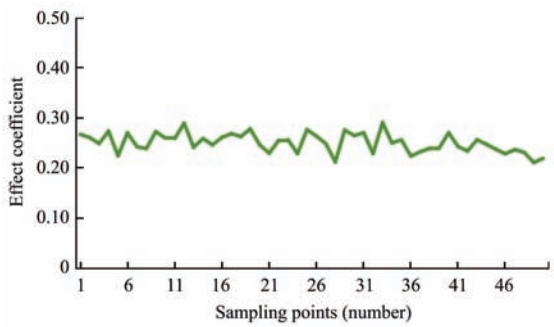

c. Broadleaf forest

Figure 7 Error coefficient of LAI for different vegetation types

3.3 Retrieval of high spatial and temporal resolution LAI product by fusing GF-1 and MODIS data

LAI varies with different vegetation types and growth seasons. In order to obtain the relationship between NDVI and LAI, it is necessary to carry out a land use and land cover (LULC) classification for the study area. In this study, the classification was conducted using a maximum likelihood supervised classification and the GF-1 image. The obtained LULC classes included farmland, broadleaf forest, grassland, built up area, water body, and bare soil (Figure 8).

The LAI values were plotted against the NDVI values from MODIS products and the models that accounted for the relationships were developed for each of the LULC types in Figure 9.

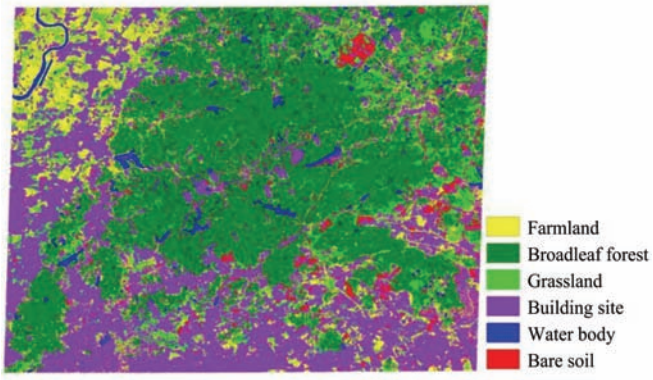

Figure 8 Land use and land cover classification map using supervised classification and GF-1 image

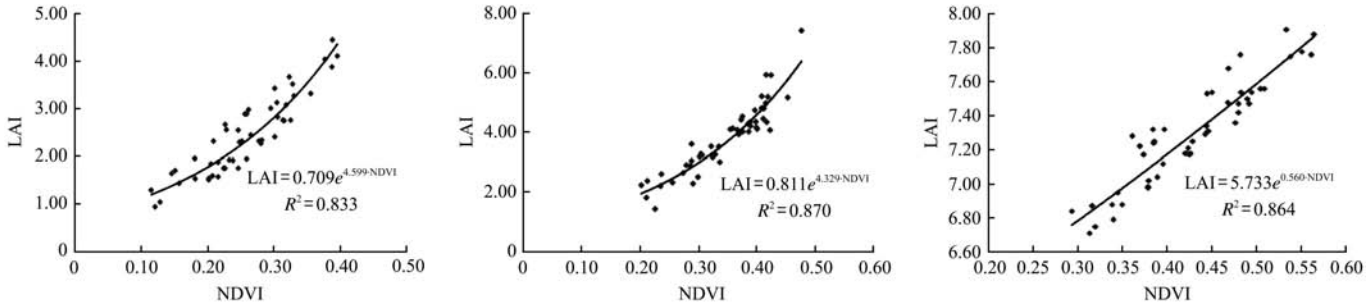

a. Farmland b. Grassland c. Broadleaf forest

Figure 9 The regression models of LAI against NDVI for different vegetation types

The results showed that the LAI tended to exponentially increase with NDVI when the determination coefficients varying from 0.833 to 0.870. The regression models can be used to estimate LAI values for different vegetation types based on the GF-1 image derived NDVI data. The obtained spatial distribution of LAI is shown in Figure 10.

Figure 10 The spatial distribution of vegetation canopy LAI using the regression models and LULC classification map based on GF-1 image derived NDVI data

3.4 High spatial and temporal resolution LAI from GF-1 and MODIS LAI data using Cressman method

The experiment showed that broadleaf forest had a larger landscape dominance index, but relatively smaller landscape fragment index than the other vegetation types. Therefore, its influence radius was the largest among three vegetation types. When the LAI was retrieved from GF-1 LAI with the method used to adapt the broadleaf forest LAI from the interpolated MODIS LAI product, the effect of adjustment was increased with the expanding of influence radius in the weighting function. In this study, the calculated influence radius of farmland, grassland and broadleaf forest were respectively 5.62 m, 3.44 m and 2.58 m. The high spatial resolution LAI images of the study area throughout year 2013 were obtained using Cressman method. The results and the dynamic change information for the MODIS LAI and the spatial information of GF-1 high resolution remote sensing observations are shown in Figure 11.

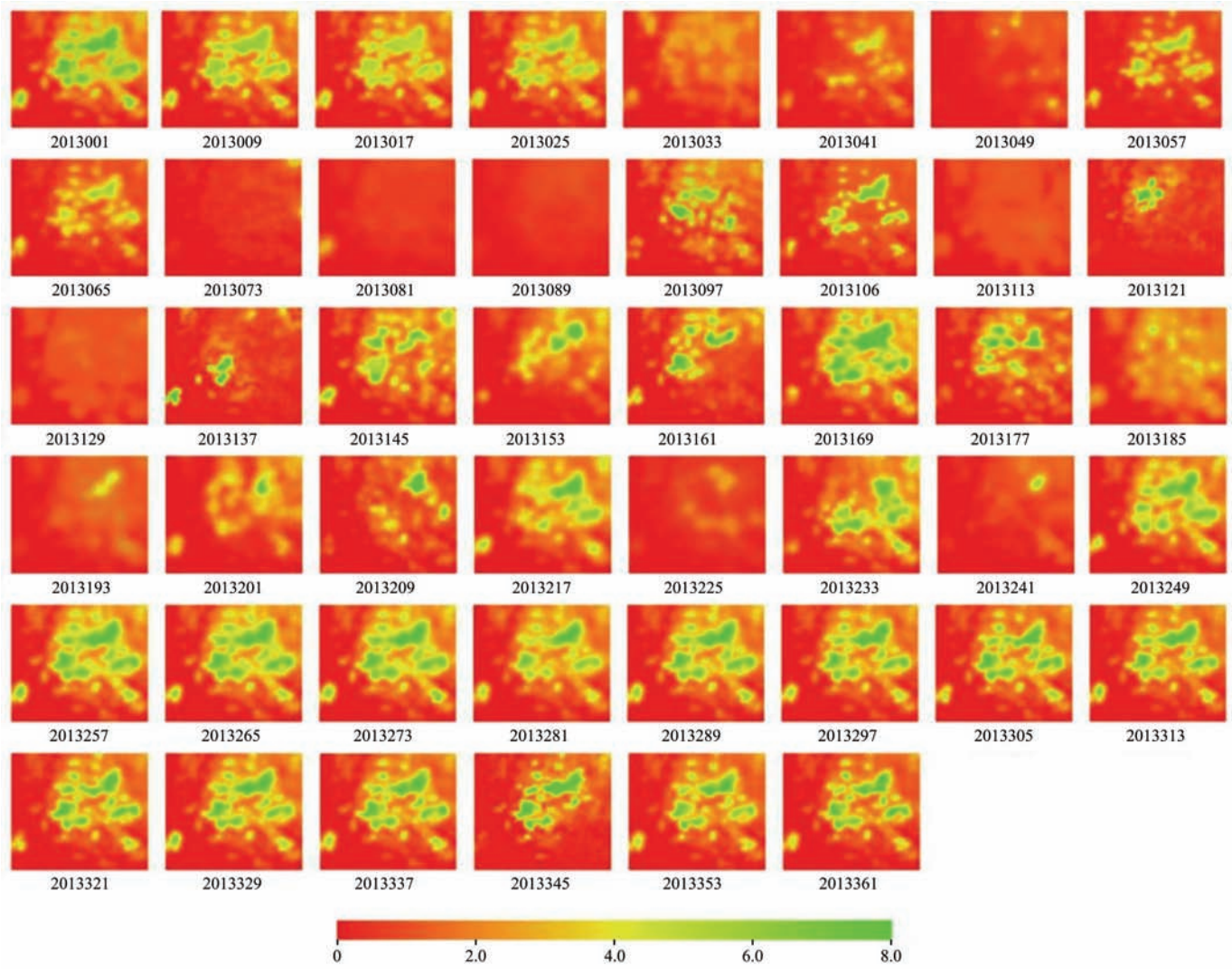

Figure 11 High spatial and temporal resolution LAI from the GF-1 and MODIS LAI data of the study area for year 2013

Figure 11 exhibits the different characteristics of dynamic changes. The smallest LAI values occurred in the late winter and spring period (February, March, April and May), while the largest LAI values appeared in January, September, October, November and December. The study area is located in the low latitude area characterized by a subtropical monsoon climate. The vegetation is evergreen and there is no significant difference between spring and autumn. Thus, the time series of LAI did not completely change with seasons defined by the climatology. Because the study area is dominated by broadleaf forests (more than 40%), it exhibited much greater effect on the trend of LAI in time series.

4 Conclusions and discussion

In this study, a novel method that combining Kriging and Cressman interpolation was proposed to generate finer spatial and temporal resolution LAI products based on MODIS and GF-1 images. This method was applied to a suburb area of Huangpu district, Guangzhou, Guangdong Province of China and led to an acceptable accuracy of 73.12% for the predicted values of LAI compared to its field observations. This implies that this method is a powerful tool to create finer spatial and temporal resolution LAI products. The Moran's I index was used to test the spatial autocorrelation of MOIDS products, while Kolmogorov-Smirnov was used to test the normal distribution of MODIS products. The results show that the MODIS data are spatially auto-correlated and characterized by normal distributions and thus meet the assumptions of Kriging. The 1 km×1 km spatial resolution MODIS products were then scaled down to a spatial resolution of 30 m×30 m using point-Kriging, which generated a precision of 79.38% compared to the results at the same spatial resolution derived from an

8 m×8 m spatial resolution GF-1 image by scaling up using block-Kriging.

The study area was classified into farmland, broadleaf forest, grassland, building site, water body and bare soil using a GF-1 image and a supervised classification procedure. For each vegetation type, a regression model that accounts for the relationship between NDVI and LAI based on MODIS data was built and then used to retrieve a GF-1 based LAI product. The regression models had acceptable accuracies with the coefficients of determination ranging from 0.833 to 0.870.

In this study, when Cressman method was used to combine MODIS and GF-1 data for generating fine spatial and temporal resolution LAI products, only one GF-1 image was used, which inevitably led to accumulative uncertainties that were unknown. In order to reduce the uncertainties, more GF-1 images should be used in the further study.

Acknowledgments

This research was supported by Science and Technology Program of Guangzhou, China (2014A050503060).

[References]

[1] Myneni R B, Hoffman S, Knyazikhin Y, Privette J L, Glassy J, Tian Y, et al. Global products of vegetation leaf area and fraction absorbed PAR from year one of MODIS data. Remote Sensing of Environment, 2002; 83(1): 214–231. DOI: 10.1016/s0034-4257(02)00074-3.

[2] Veroustraete F, Patyn J, Myneni R B. Estimating net ecosystem exchange of carbon using the normalized difference vegetation index and an ecosystem model. Remote Sensing of Environment, 1996; 58(1): 115–130. DOI: 10.1016/0034-4257(95)00258-8.

[3] Huang H P. Scale issues in object-oriented image analysis. Beijing: Graduate University of Chinese Academy of Sciences, 2003. (in Chinese with English abstract)

[4] Zhou M, Zhang J L. Review on scale transformation for remote sensing image and selection of optimal spatial resolution. World Nuclear Geoscience, 2011; 28(2): 94–98. (in Chinese with English abstract)

[5] Wang Q L. Study on object-oriented remote sensing image classification and its application-taking urban vegetation extraction in Futian, Shenzhen city for example. Nanjing: Nanjing Forestry University, 2008. (in Chinese with English abstract)

[6] He M. Land use information extraction by object-oriented technology based on remote sensing image. Sichuan: Southeast University of Science and Technology, 2006. (in Chinese with English abstract)

[7] Guo L M. An analysis on scale transformation in remote sensing-based on fractal theory. Shaanxi: Southwest University, 2008. (in Chinese with English abstract)

[8] Hay G J, Niemann K O. Spatial thresholds, image-objects, and up scaling: a multi-scale evaluation. Remote Sensing of Environment, 1997; 62(1): 1–19. DOI: 10.1016/s0034-4257(97)81622-7.

[9] Atkinson P M, Tate N J. Spatial scale problems and geostatistical solutions: A review. The Professional Geographer, 2000; 52(4): 607–623. DOI: 10.1111/0033-0124.00250.

[10] Crow W T, Ryu D, Famiglietti J S. Upscaling of field-scale soil moisture measurements using distributed land surface modeling. Advances in Water Resources, 2005; 28(1): 1–14. DOI: 10.1016/j.advwatres.2004.10.004.

[11] Famiglietti J S, Devereaux J A, Laymon C A, Tsegaye T, Houser P R, Jackson T J, et al. Ground-based investigation of soil moisture variability within remote sensing footprints during the Southern Great Plains 1997 (SGP97) Hydrology Experiment. Water Resources Research, 1999; 35(6): 1839–1851. DOI: 10.1029/1999wr900047.

[12] Mohanty B P, Skaggs T H. Spatio-temporal evolution and time-stable characteristics of soil moisture within remote sensing footprints with varying soil, slope, and vegetation. Advances in Water Resources, 2001; 24(9): 1051–1067. DOI: 10.1016/s0309-1708(01)00034-3.

[13] Cosh M H, Jackson T J, Bindlish R, Prueger J H. Watershed scale temporal and spatial stability of soil moisture and its role in validating satellite estimates. Remote Sensing of Environment, 2004; 92(4): 427–435. DOI: 10.1016/j.rse.2004.02.016.

[14] Li H B, Lin Z H, Liu S X. Application of Kriging technique in estimating soil moisture in China. Geographical Research, 2001; 22(5): 472-478. (in Chinese with English abstract)

[15] Zhang J G, Chen H S, Su Y R, Zhang W, Kong X L. Spatial variability of soil moisture in surface layer in depressed karst region and its scale effect. Acta Pedologica Sinica, 2008; 45(3): 544–549. (in Chinese with English abstract)

[16] Grayson R B, Western A W. Towards areal estimation of soil water content from point measurements: time and space stability of mean response. Journal of Hydrology, 1998; 207(1): 68–82. DOI: 10.1016/s0022-1694(98)00096-1.

[17] Woodcock C E, Strahler A H. The factor of scale in remote

sensing. Remote Sensing of Environment, 1987; 21(3): 311–332. DOI: 10.1016/0034-4257(87)90015-0.

[18] Doraiswamy P C, Sinclair T R, Hollinger S, Akhmedov B, Stern A, Prueger J. Application of MODIS derived parameters for regional crop yield assessment. Remote Sensing of Environment, 2005; 97(2): 192–202. DOI: 10.1016/j.rse.2005.03.015.

[19] Liu Y. Atmospheric correction on MODIS satellite image based on FLAASH model. Geomatics & Spatial Information Technology, 2013; 36(3): 47–49. (in Chinese with English abstract)

[20] Goovaerts P. Geostatistics for natural resources evaluation. Oxford University Press, 1997.

[21] Cressie N. Statistics for spatial data. Revised Edition. John Wiley & Sons, Inc. 2015; pp.149-165.

[22] Kyriakidis P C. A geostatistical gramework for area-to-point spatial interpolation. Geographical Analysis, 2004; 36(3): 259–289. DOI: 10.1111/j.1538-4632.2004.tb01135.x.

[23] Yuan H, Dai Y J, Xiao Z Q, Wei S G. Reprocessing the MODIS Leaf Area Index products for land surface and climate modelling. Remote Sensing of Environment, 2011; 115(5): 1171–1187. DOI: 10.1016/j.rse.2011.01.001. (in Chinese with English abstract)

[24] Wang Q C, Zhang X H, Zhang L Y, Niu S K. Forest landscape diversity of Labagoumen Nature Reserve in Beijing. Journal of Beijing Forestry University, 2002; 24(3): 54–60. (in Chinese with English abstract)

[25] Lu P, Peng P Q, Song B L, Tang G Y, Zou Y, Huang D Y, Xiao H A, Wu J S, Su Y R. Geostatistical and GIS analyses on soil total P in the typical area of Dongting Lake plain. Scientia Agricultura Sinica, 2005; 38(6): 1204–1212.

[26] Mao S S, Cheng Y M, Pu X L. Probability & Statistics (The Second Edition). Beijing: China Higher Education Press.

[27] Zheng Y, Chen T, Chen H, Wu H, Zhou J, Luo J, et al. The spatial structure and distribution of Ni contents in soils of suburbs of Beijing. Acta Geographica Sinica, 2003, 58(3): 470–476. (in Chinese with English abstract)

[28] Peng X, Zhang S W. Research on rice growth status based on NDVI and LAI. Remote Sensing Technology and Application, 2002; 17(1): 12–15. (in Chinese with English abstract)

[29] Wang F M, Huang J F, Tang Y L, Wang X Z. Estimation of rice LAI using NDVI at different spectral bandwidths. Chinese Journal of Applied Ecology, 2007; 18(11): 2444–2450. (in Chinese with English abstract)

[30] Gan Y W, Cheng P, Zhou C B, Luo Y J, Kuang Y, Zhang X H. Study on pertinence between the vegetation indexes and the aboveground biomass of Sub-alpine meadow of Zoige County. Journal of Natural Resources, 2009; 24(11): 1963–1972. (in Chinese with English abstract)